JOURNAL OF MAGNETIC RESONANCE **132,** 298–306 (1998)
ARTICLE NO. MN981390

# Multivariate Image Analysis of Magnetic Resonance Images with the Direct Exponential Curve Resolution Algorithm (DECRA)

## Part 1: Algorithm and Model Study

W. Windig,[1] J. P. Hornak,* and B. Antalek

*Imaging Research and Advanced Development, Eastman Kodak Company, Rochester, New York 14650-2132; and*
**Center for Imaging Science, Rochester Institute of Technology, Rochester, New York 14623-5604*

E-mail: windig@kodak.com

Received July 28, 1997; revised December 22, 1997

**Antalek and Windig recently presented a fast method to resolve a series of NMR mixture spectra, where the contribution of the components varies with a decaying exponential [B. Antalek and W. Windig,** *J. Am. Chem. Soc.* **118, 10,331–10,332 (1996); W. Windig and B. Antalek,** *Chemom. Intell. Lab. Syst.* **37, 241–254 (1997)]. The method was called DECRA (direct exponential curve resolution algorithm). In this paper DECRA will be applied to two series of magnetic resonance images. The signal of one series is based upon $T_2$ relaxation, and the other is based upon $T_1$ relaxation. In order to evaluate the technique, the magnetic resonance images of a phantom where used. A transformation is introduced to enable the application of DECRA to a $T_1$ series of magnetic resonance images. A separate paper in this issue will describe the application of the techniques to magnetic resonance images of the human brain.**



*Key Words:* **MRI; multivariate image analysis; exponentials; $T_1$ relaxation; $T_2$ relaxation.**

### INTRODUCTION

Antalek and Windig recently showed that a series of NMR spectra where the contribution of the components varies with a decaying exponential profile can be resolved fast and accurately. The newly developed method is called DECRA (direct exponential curve resolution algorithm), and it is based on the general rank annihilation method (GRAM) (*1, 2*). The algorithm assumes the presence of two mixture data sets with a proportional behavior between the elements of the set. The spectra of the pure components are identical and the concentrations are identical, but they differ with a scale factor, which is different for each of the components. In mathematical terms, this relation can be expressed as follows:

$$A = CP^T \quad [1]$$

$$B = C\alpha P^T. \quad [2]$$

A and B are data matrices of size $s \times v$; $s$ is the number of spectra and $v$ is the number of variables (i.e., real data points in each spectrum). $C$ (size $s \times n$) and $P$ (size $v \times n$) are the concentration and pure spectra matrices of $n$ components. The matrix $\alpha$ is a diagonal matrix (size $n \times n$), of which all the elements have a different value. In these two data sets the pure spectra and the concentrations are proportional; they only differ by a certain scaling factor as defined by the diagonal matrix $\alpha$.

Kubista showed that it is possible to resolve mixtures of two data sets unambiguously (*3, 4*). Booksh and Kowalski showed that Kubista's method can be expressed in terms of GRAM, which eliminates some problems and restrictions with Kubista's method (*5*). For details about the GRAM algorithm, see (*6, 7*).

Traditionally, the two data sets have been obtained by analyzing two samples with the relation just described, or by applying two different experiments to one sample where the different experiments create the proportional relation. In both cases, two experiments are performed. Exponential profiles, however, have a property that makes it possible to apply GRAM to a single experimental data set by simply using two different parts of the data set. In order to demonstrate the property of decaying exponentials involved, an example of two exponential decays is given in Table 1. D represents a data set of which the exponentially decaying concentration profiles of two components ($n = 2$) are given in the first and second column under D. The data in the first column have a faster decay rate than the data in the second column. Data set D is split into two data sets A and B. The data set A is created using the first three ''spectra'' of

[1] To whom correspondence should be addressed. Fax: (716) 477-7781.



1090-7807/98 $25.00

**TABLE 1**
**Representative Signal Decay Data**

| D | | A | | B | |
|---|---|---|---|---|---|
| Component 1 | Component 2 | Component 1 | Component 2 | Component 1 | Component 2 |
| 27 | 8 | 27 | 8 | 9 | 4 |
| 9 | 4 | 9 | 4 | 3 | 2 |
| 3 | 2 | 3 | 2 | 1 | 1 |
| 1 | 1 | | | | |

data set D, and data set B is created by using the last three spectra of data set D. For both A and B, $s = 3$ and $v = 2$. Because of the exponential character of the profiles, the first column of A is a constant (3) times the first column of column B, and the second column of A is a constant (2) times the second column of B. As a consequence, the data sets A and B fulfill the requirements as expressed in Eqs. [1] and [2]. In this case the matrix $\alpha$ in Eq. [2] contains 0.33 and 0.50 as diagonal elements. This means that in the case of exponentially decaying functions, one can use two different parts of the data set to create the two data sets necessary to apply Kubista's method or GRAM.

*PGSE NMR Spectra*

DECRA was applied to a series of pulsed gradient spin echo (PGSE) NMR spectra of which the exponential decay in the series of spectra is based on the diffusivities of the different components (*1, 2*). Using the standard spin echo version of the PGSE NMR experiment (*8*) the relationship of the acquired signal S from component *i* to the diffusion coefficient *D* of component *i* is described by

$$S_i \propto e^{-D_i(\gamma g \delta)^2(\Delta - \delta/3)}. \qquad [3]$$

$\gamma$ is the gyromagnetic ratio and $\Delta$ and $\delta$ are timing parameters in the pulse sequence. Spectra are collected by varying the magnetic field gradient $g$. The spectra of the pure components and their contributions (''concentrations'') in the original mixture spectra are extracted. The diffusivities derived from the exponentials were accurate.

*Magnetic Resonance Images*

The exponential profiles necessary to apply DECRA are also present in a series of magnetic resonance (MR) images whose signal depends upon the spin–spin relaxation $T_2$ or the spin–lattice relaxation $T_1$ (for which a transformation is needed and will be introduced later). Using the standard single-slice, single-echo, spin-echo sequence and assuming that the repetition time TR is much larger than the echo time TE, the signal $S$ of a component $i$ is described by

$$S_i \propto \sum_i \rho_i e^{-\mathrm{TE}/(T_2)_i}(1 - e^{-TR/(T_1)_i}), \qquad [4]$$

where $\rho$ is the spin density. Varying TE and keeping TR constant or vice versa will result in a series that depends upon $T_2$ or $T_1$, respectively. Because of the chemical nature and physical environments of the $^1$H nuclei (described by their relaxation behavior) a series of these $T_2$ (or $T_1$) images can be considered as a mixture of images. Each component of the mixture presents an image defined by a single exponential with time constant $T_2$ (or $T_1$). As a consequence, it is possible to extract the pure $T_2$ (or $T_1$) images. The analogy between the spectra and the images is summarized next.

The PGSE NMR data set comprises a series of mixture spectra of chemical components characterized by different exponential decays that depend on diffusivities. DECRA calculates the spectra of the pure chemical components and their contributions (concentrations) in the original spectra. The profiles formed by the contributions of a single chemical component over the whole series of spectra are exponential. From the derived exponentials the diffusivities are obtained.

The magnetic resonance image data set is comprised of a series of mixture images of $^1$H environments characterized by different exponential decays that depend on spin–spin (or spin–lattice) interactions. DECRA calculates the images of the pure $^1$H environments and their contributions (concentrations) in the original images. The profiles formed by the contributions of a single $^1$H environment over the whole series of images are exponential. From the derived exponentials the $T_2$ (or $T_1$) values are obtained.

The analysis of a series of images with interimage variation is the subject known as multivariate image analysis (MIA) (*9*). Using principal component analysis (PCA), it is generally possible to reduce a series of related images to a small number of images that contain all the original information. Since the images resulting from PCA are based on mathematical criteria, they may exhibit positive and negative intensities. An offset needs to be added to display the

PCA results as images. Examples have been shown for satellite images (*10–12*) and MR images (*13–15*). Multivariate analysis is normally used in cases where every object (in our case an image) is an array. A series of objects forms a matrix, which is a two-way array. In MIA the object is an image, and a series of images forms a three-way array. In order to be able to apply PCA (or a technique such as DECRA), each image is reorganized into an array by appending the rows or columns of pixels.

The pixel intensities of the two or three PCA images can be plotted against each other, and clusters in such a presentation can be selected to enhance certain features in the images. This process is called segmentation (*9*). Furthermore, regression of the extracted images can be applied to certain highlighted parts of the images in order to enhance, for example, certain tissue types in MR images (*15*).

Instead of the mathematically determined images resulting from PCA, it is also possible to plot the pixel intensities of more ''natural'' images and obtain segmentation. This is done using an iterative fitting procedure to a single exponential function on registered pixels within the entire image series. This is the approach of Fletcher *et al.* (*16*), who used $T_1$, $T_2$ (derived from the fitted exponentials) and spin density ($\rho$) weighted images.

This paper shows the application of DECRA to both a series of images that are related to $T_2$ and a series of images that are related to $T_1$. A transformation of a $T_1$ series of images will be introduced that makes it possible to apply DECRA. An important difference between Geladi's method (*9*) and DECRA is that Geladi's method extracts images that are abstract, because of the use of PCA, whereas the extracted images of DECRA relate to certain $^1$H environments defined by their $T_1$ or $T_2$ behavior. In order to show the feasibility of the method, phantom images will be used, so that the information provided by DECRA can be compared with the known composition. A separate paper will describe applications of DECRA to $T_1$ and $T_2$ images of the human brain (*17*).

## MATERIALS AND METHODS

### *Algorithm*

This section will show the algorithm used for the analysis of the data presented in this paper. It is based on the paper of Sanchez and Kowalski (*6*).

Equations [1] and [2] can be rewritten as

$$C = A(P^T)^+ \quad [5]$$

$$C\alpha = B(P^T)^+, \quad [6]$$

where $(P^T)^+$ represents the pseudoinverse of the matrix $P^T$.

Post-multiplying the left and right side of Eq. [5] by $\alpha$ results in

$$C\alpha = A(P^T)^+\alpha. \quad [7]$$

Combining Eqs. [6] and [7] results in

$$A(P^T)^+\alpha = B(P^T)^+. \quad [8]$$

This can be rewritten as

$$AZ\alpha = BZ, \quad [9]$$

where

$$Z = (P^T)^+. \quad [10]$$

The expression in Eq. [9] is known as the generalized eigenvector problem, where $Z$ contains the eigenvectors and $\alpha$ contains the eigenvalues. The decay values can be calculated directly from the eigenvalues. In order to solve the generalized eigenvector problem, the matrices $A$ and $B$ need to be square. This can be achieved by projecting $A$ and $B$ in a common PCA space (*2*).

In order to be able to apply the algorithm to the images,

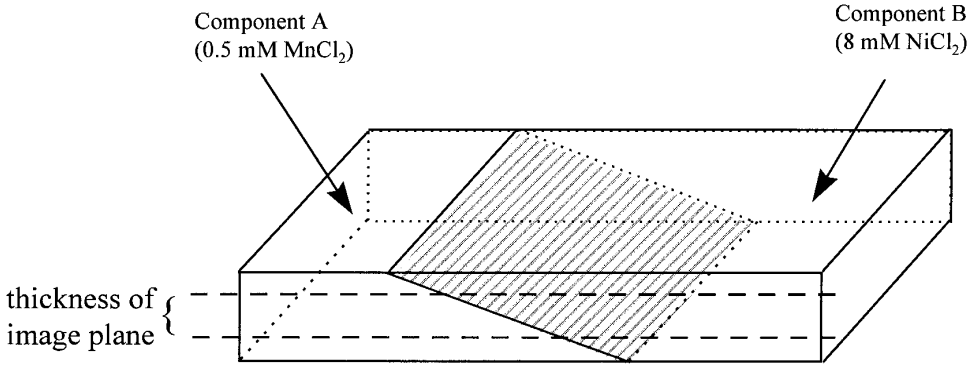


**FIG. 1.** A schematic representation of the phantom used for this study.

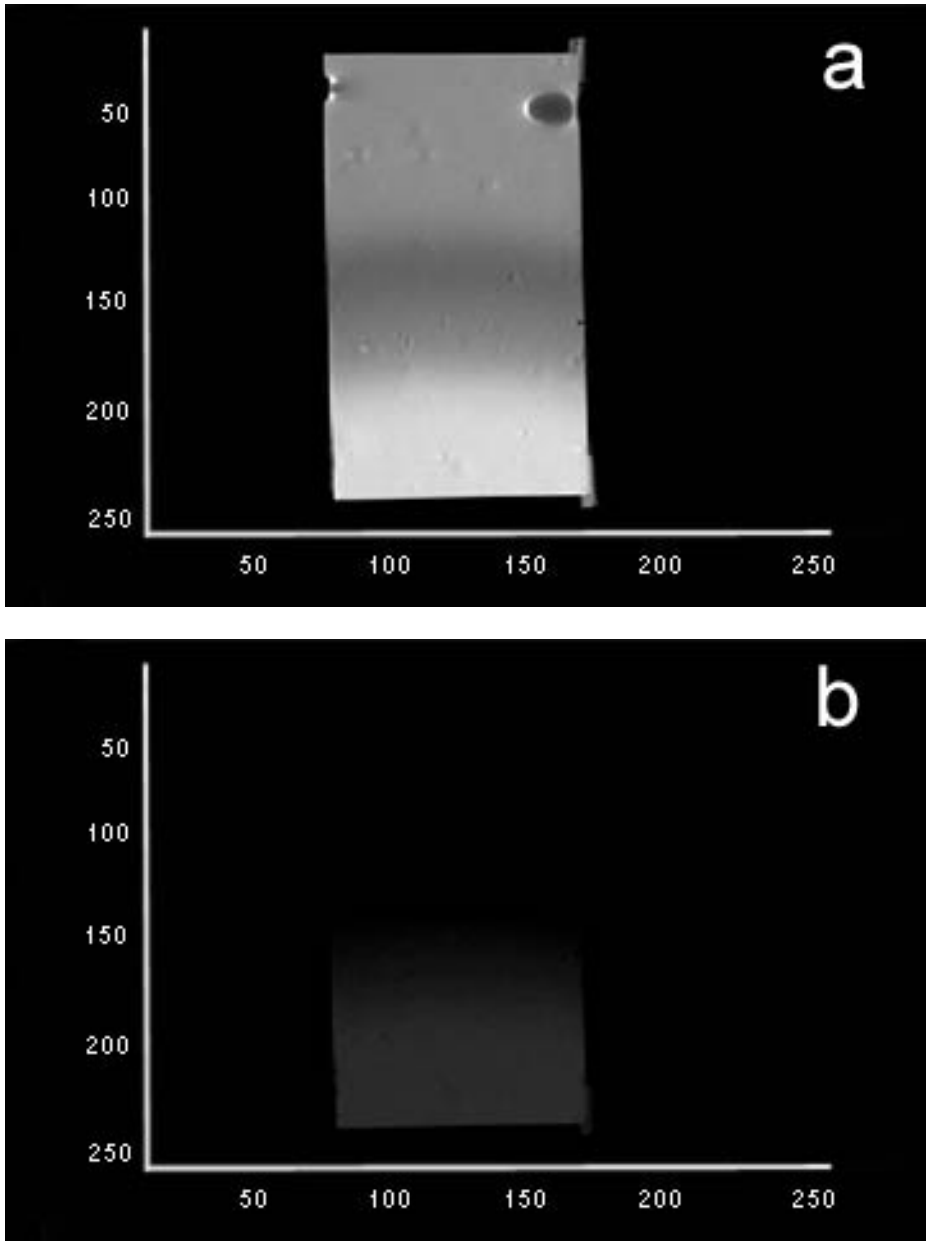


**FIG. 2.** (a) The first image of the $T_2$ series. It is basically a top view of the phantom in Fig. 1. An air bubble can be observed at the pixel coordinates of approx. 160, 40. (b) The last image of the $T_2$ series.

the images were reorganized into arrays, and the arrays into a data matrix. For example, a series of 10 256 × 256 images results in a 10 × 65536 data matrix.

*$T_1$ Transformation*

For this section, Eq. [4], with constant TE, is simplified as follows:

$$a_1(1 - e^{-bx}). \qquad [11]$$

This function does not show the proportional behavior of the exponential as described in Table 1, and the DECRA technique cannot be applied. If the term $a_1$ is known, it would be simple to subtract this constant. Because $a_1$ is not known, a subtraction procedure is not a viable option. However, a simple mathematical procedure can be applied to make it possible to use DECRA. Equation [11] can be rewritten as

$$a_1(e^{0x} - e^{-bx}). \qquad [12]$$

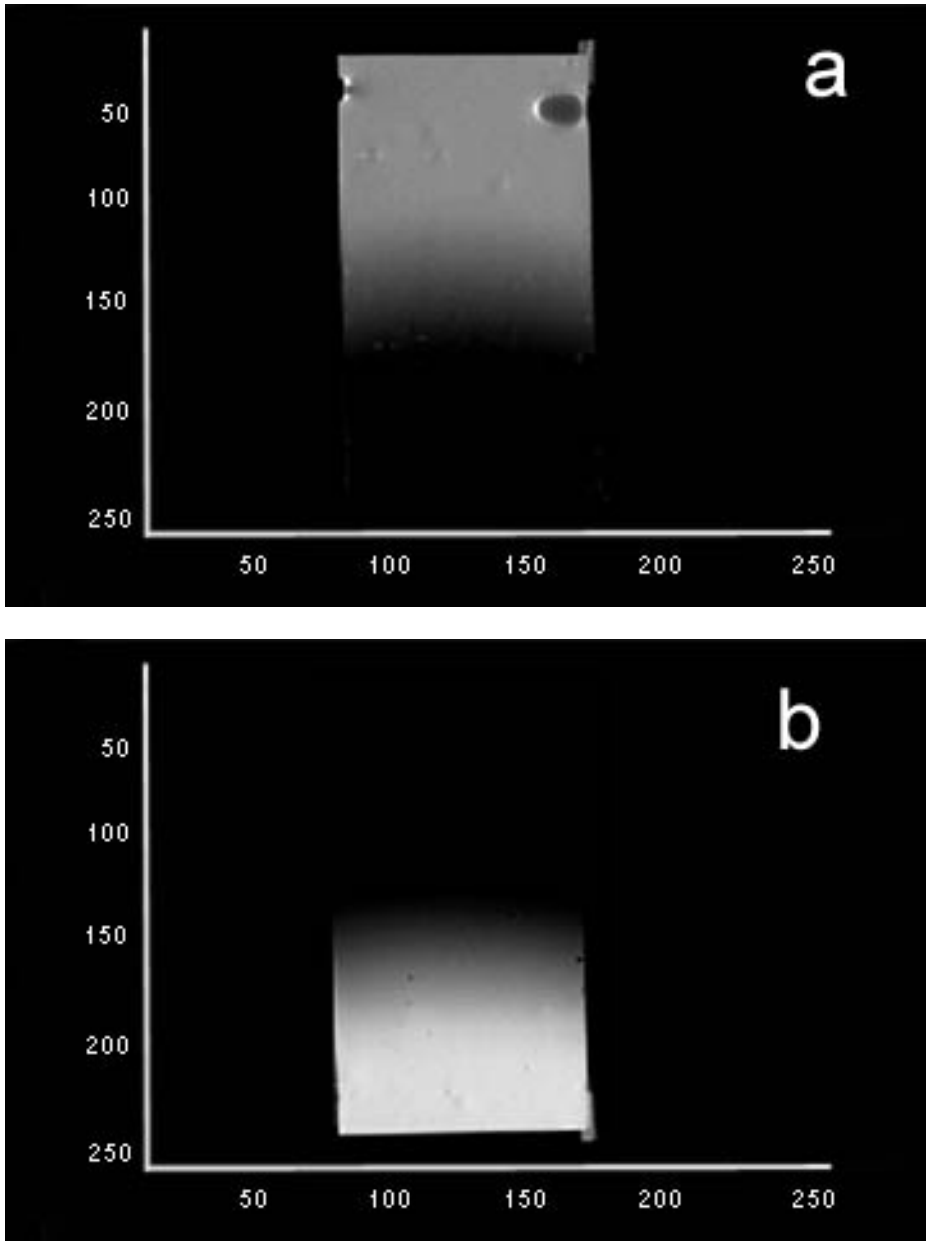


**FIG. 3.** (a) The resolved component of $MnCl_2$ compartment and (b) the resolved component of the $NiCl_2$ compartment.

This shows that the expression basically is a linear combination of two exponential functions. This ''data set'' cannot be resolved using DECRA, because we have two exponentials in a data set of rank 1 (i.e., the number of *linearly independent* components is 1). However, since one of the exponentials is known, $e^{0x}$, it is possible to add this as a new component to the data set in the form of an extra variable. This can be extended to complete data sets of $T_1$ character and basically consists of adding a column to the data set where all the elements have a constant value. Simulated data sets were used to confirm this surprisingly simple procedure.

In practice, it appeared that the resolved data of $T_1$ images were relatively noisy. By applying singular value decomposition to the data set prior to adding the column with constant values, and reproducing the data set using ncom singular values, where ncom represents the number of components in the data set (2 for the phantom), the noise was reduced significantly.

### *Imaging*

A simple phantom was constructed to test DECRA and shown in Fig. 1. It consists of a plastic [PVC, poly(vinyl chloride)] box having the dimensions 18 cm $\times$ 10 cm $\times$ 1

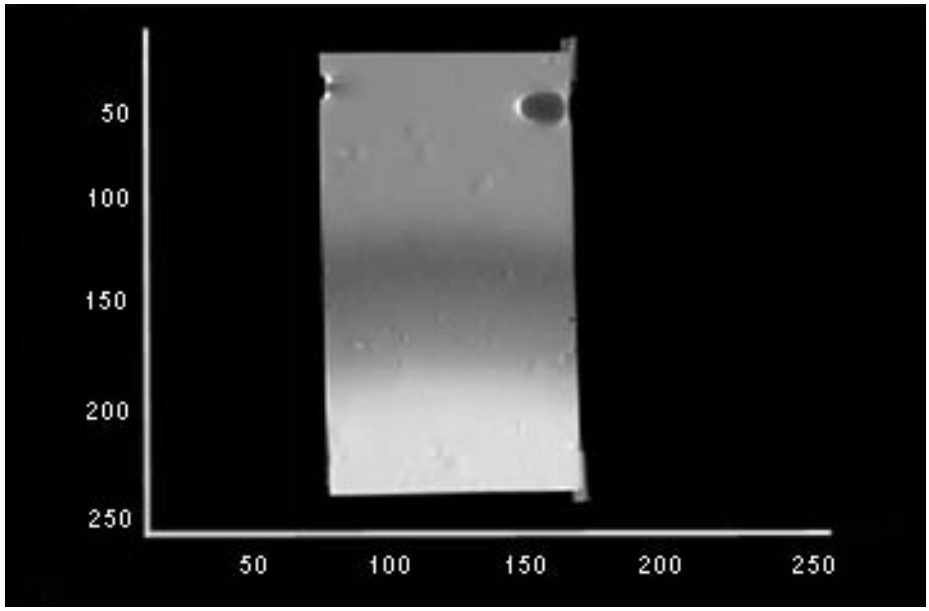


**FIG. 4.** The reconstructed first image of the $T_2$ series.

cm, and containing two compartments separated by a thin plastic (PVC) sheet of thickness, 0.18 cm. The compartments, therefore, formed two wedge-shaped spaces. The angle of the wedge is 6.2°. These spaces were filled with water that contained a specific amount of paramagnetic salt. One space contained 0.5 mM $MnCl_2$ and the other 8 mM $NiCl_2$. These concentrations were chosen to provide water $T_2$ values of near 30 and 150 ms, respectively. The plastic separation sheet was glued to completely seal one compartment from the other. The solution containing the $MnCl_2$ salt will be designated component A and that containing the $NiCl_2$ salt component B. Component A will be depicted toward the left side of the figures.

A GE Signa 1.5-T whole body imager employing a standard spin-echo pulse sequence and standard birdcage RF coil was used for all of the image acquisition. For the phantom 15, 256 × 256 pixel, images were acquired of a 5-mm thick plane passing through the long axes of the object and parallel to the 18 cm × 10 cm surfaces. The image plane is represented in Fig. 1 with a dashed line. The parameter, TE, in the spin echo pulse sequence (see Eq. [1]) was varied starting at 15 milliseconds (ms) and incremented by 15 ms for each image. TR was a constant of 2000 ms and the field of view was 20 cm. Varying TE resulted in a dependence in signal intensity for each image based upon $T_2$ relaxation. The phantom was constructed so that one may obtain, using a 5-mm slice thickness, an image with three general regions, two regions where the signal represents the pure decay behavior of each component (close to the ends) and a middle region which represents a weighted sum of the two.

For the $T_1$ image series the same experimental procedure and parameters were used, except that 10 images were acquired with a fixed TE of 15 ms and a TR starting at 200 ms and incremented by 200 ms.

### *Data Analysis*

For the data analysis MATLAB software was used (The MathWorks, Inc., Natich, MA 01760). The computer configuration is a Pentium, 90 MHz, 64 MB RAM.

## RESULTS AND DISCUSSION

### *$T_2$ Image Series*

Figure 2 shows the first and last image of the $T_2$ image series. The top of each image in Fig. 2 shows the contribution of only the compartment with $MnCl_2$, and the bottom of each image shows the contribution of only the compartment with $NiCl_2$. In the middle region the signal is a mixture of the two compartments. The intensity is lower in the middle because of the presence of the divider. Comparing Figs. 2a and 2b, it is clear that the $MnCl_2$ compartment has the fastest decay rate. The data set was split into two parts for DECRA: images 1−14 for the first part and images 2−15 for the second part. The calculations take 40 s. The output of DECRA (after reorganizing the output into images) using two components is given in Fig. 3. The two components clearly describe the phantom structure. In order to verify that using two components describes the original data set appropriately, the first image was reconstructed from the resolved results. The reconstructed image in Fig. 4 is indistinguishable from the original image in Fig. 2a.

When using three components for DECRA, the extra component extracted clearly represents noise, which is similar

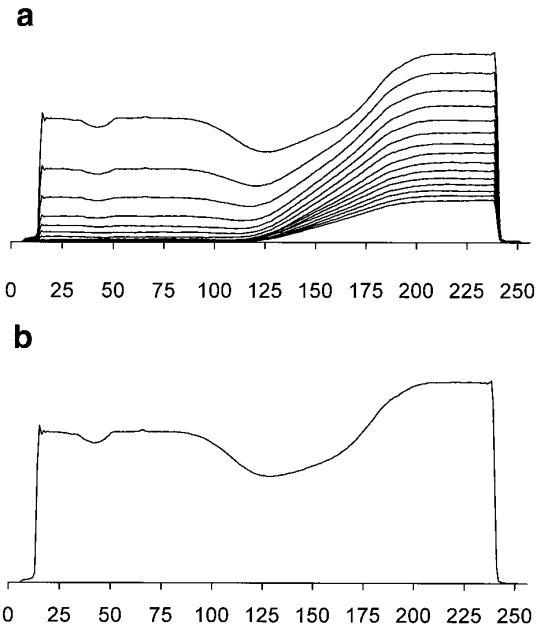


**FIG. 5.** (a) Image profiles of the $T_2$ series; (b) standard deviation of the image profiles in (a).

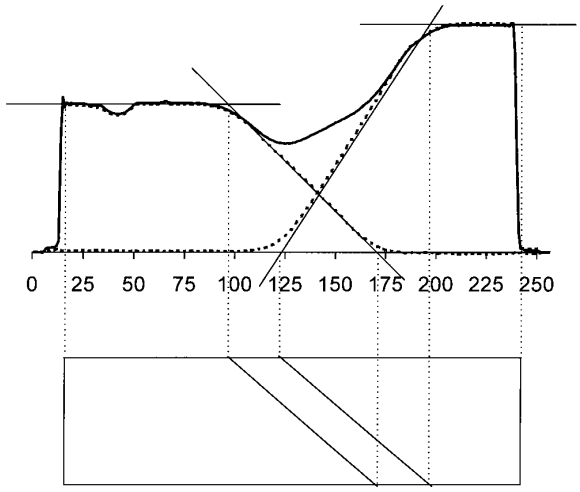


**FIG. 6.** The resolved image profiles (dashed lines) for the first image, the sum of the resolved image profiles (solid line), and the original image profile (dashed line; cannot be distinguished from solid line). In order to see the relation with the original sample, the phantom is reconstructed from the image profiles.

to the experience with spectra (*2*): The contribution profile was negative and the image, dominated by noise, had negative intensities which were in the same range as the positive intensities. This clearly indicates that the data set has two components.

In order to judge the images more objectively, ''image profiles'' are plotted. An image profile is obtained by averaging the columns of an image between *x* pixel positions 77 and 165. The original data can now be plotted in a single figure (see Fig. 5a). In order to check the quality of the data set, the standard deviation image profile of the original data set is given in Fig. 5b. As expected, the areas in the phantom where the pure components can be observed (approximately from pixel position 20 to 100 and from pixel position 200 to 240) is horizontal. The image profiles in Fig. 5 show a dip in intensities between pixel positions 100 and 200, which is due to the thickness of the screen that separates the two compartments, and which gives no signal.

In Fig. 6, the image profiles of the two resolved components are given. These image profiles are scaled to reproduce the first image. The dashed line that increases between pixel positions 125 and 200 represents the $NiCl_2$ compartment of the phantom, and the dashed line that decreases between pixel positions 100 and 175 represents the $MnCl_2$ compartment of the phantom. The sum of the two image profiles is represented by a solid line. In order to show how well the original image has been reproduced, the image profile of image 1 is also given with a dashed line. Because of the high overlap, it cannot be distinguished from the sum of the two resolved image profiles.

In order to show the relation of the resolved image profiles with the phantom, the phantom was reconstructed from the data resolved image profiles; see Fig. 6.

The contribution profiles of the $T_2$ phantom are shown in Fig. 7. The contributions from the first part of the split data (images 1–14) set is plotted using ×'s. The contributions for the second part of the split data set (images 2–15) is calculated by multiplying the contribution profile of the first data set by its eigenvalue and are plotted using □'s. Because of the way the data set was split, the two profiles have an overlapping, proportional profile. It is clear from the plots in Fig. 7 that the assumption of proportionality was correct. The solid line in this figure is calculated from the eigenvalues and shows excellent fit. The $T_2$ values obtained from the eigenvalues are 28.2 ms for $MnCl_2$ (target value 29.6 ms) and 137.7 ms for $NiCl_2$ (target value 150 ms).

The high quality of these results indicate that fewer images may produce similar results. It is possible to use only three images (the minimum required for the algorithm) and still

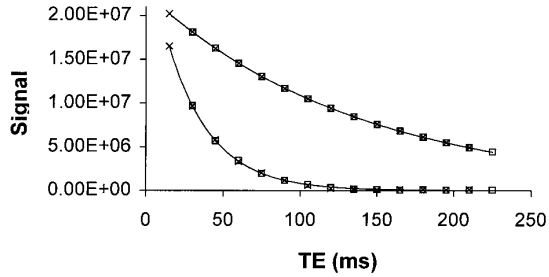


**FIG. 7.** The contribution profiles of the faster decaying $MnCl_2$ compartment and the slower decaying $NiCl_2$ compartment.

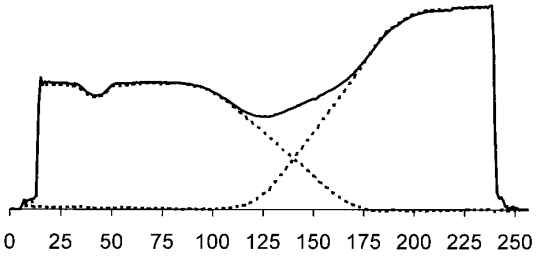


**FIG. 8.** The resolved image profiles (dashed lines) for the first image, the sum of the resolved image profiles (solid line), and the original image profile (dashed line; cannot be distinguished from solid line) using only three images.

obtain the correct results (see Fig. 8 and 9). The calculated $T_2$ values are 29.0 ms for $MnCl_2$ (target value 29.6 ms) and 136.9 ms for $NiCl_2$ (target value 150.0 ms). The calculation time was less than 3.5 s.

### *$T_1$ Image Series*

The image profiles of the $T_1$ image series and its standard deviation image profile are shown in Fig. 10. The standard deviation image profile shows that the pure regions for each of the compartments (pixel positions 15–77 and pixel positions 175–240) are not horizontal as in the standard deviation image profile of the $T_2$ images in Fig. 5, although the standard deviation values in each of the pure regions should be constant. The intensities are increasing toward the screen that separates the two compartments. Furthermore, the standard deviation image profile of the $T_1$ series is less smooth than of the $T_2$ series in Fig. 5, which indicates a higher noise level.

In order to resolve the $T_1$ data set, a column with constant values was added to the data set. This results in an extra image, which can be ignored. In order to obtain the contribution profiles from the images with the original data set, the resolved images were regressed against the original data set, similar to Eq. [3].

The data set was split into two parts: images 1–9 and images 2–10. The two images resulting from the DECRA

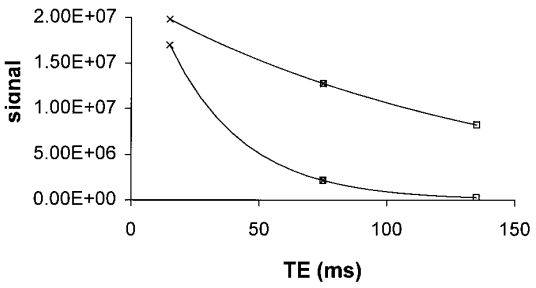


**FIG. 9.** The contribution profiles of the faster decaying $MnCl_2$ compartment and the slower decaying $NiCl_2$ compartment. Only three images are used in the analysis.

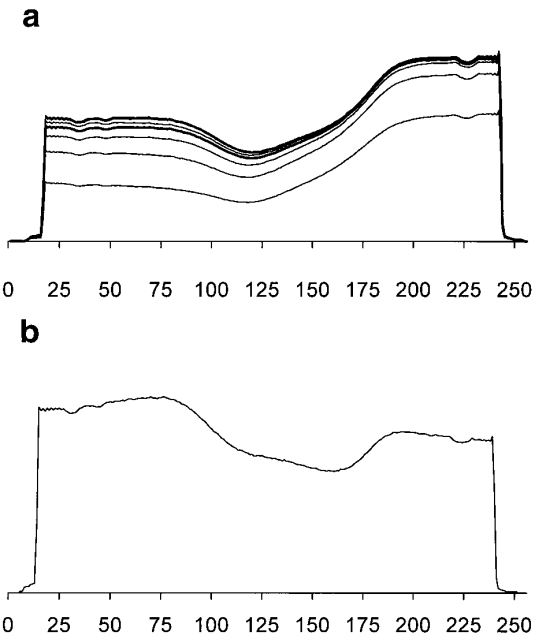


**FIG. 10.** (a) Image profiles of the $T_1$ series; (b) standard deviation of the image profiles in (a).

analysis (after ignoring the third introduced component) are shown in Fig. 11. The calculations took 45 s. Deviations from the ideal behavior can be observed, which is not so surprising, considering the deviations in the original data set. Nevertheless, the resolved image profiles are close to the expected profiles. Despite the deviations, the sum of the resolved profiles, scaled to reconstruct the 10th image, again cannot be discriminated from the original image profile.

Selecting an extra component in DECRA resulted in an image and corresponding contribution profile that were dominated by noise. This result shows clearly that the proper number of components is two.

Figure 12 shows the resolved contribution profiles, which show the expected exponential behavior. The $T_1$ values derived from the eigenvalues were 157.25 ms for $NiCl_2$ (target value: 159 ms) and 304.59 ms for $MnCl_2$ (target value: 319 ms).

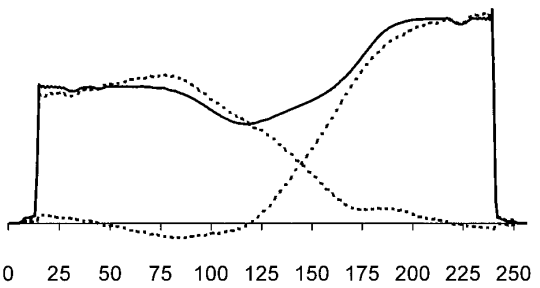


**FIG. 11.** The resolved image profiles (dashed lines) for the first image, the sum of the resolved image profiles (solid line), and the original image profile (dashed line; cannot be distinguished from solid line).

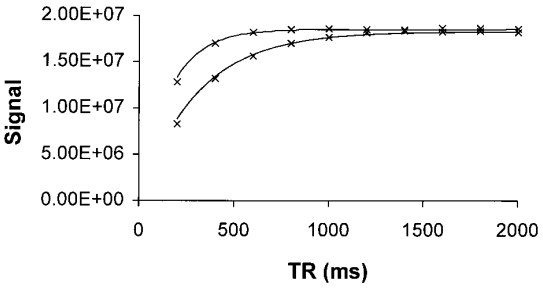


**FIG. 12.** The contribution profiles of the slower recovering compartment and the faster recovering $NiCl_2$ compartment.

It appeared that the reduction of the number of images to obtain correct results for this $T_1$ series was not as drastic as for the $T_2$ series. The minimum number of images to obtain correct results is five (instead of three for the $T_2$ series). Because of the problems that can be observed in the original $T_1$ data, more experiments are necessary for optimization.

## CONCLUSIONS

It was shown that $T_2$ images can be resolved successfully using the DECRA approach in 40 s. Using the minimum number of three images required for the algorithm, correct results were obtained in 3.5 s. Since MATLAB is an interpreter, it can be expected that a compiled version of the algorithm will be significantly faster. In order to resolve a $T_1$ series of images, a simple transformation was necessary. The transformed $T_1$ series of images could be resolved successfully using the DECRA approach, although deviations from the ideal behavior could be observed in the original data, which also affected the resolved results. The analysis time for the $T_1$ series was 45 s. The $T_1$ series could not be reduced as dramatically as the $T_2$ series, which is probably due to the higher amount of noise in the data. A separate article shows the practical applications of the techniques discussed earlier to MR images of the human brain (*17*). Further studies will include a further optimization of the $T_1$ experiment and a systematic study of how other algorithms for resolving exponential profiles compare with DECRA.

## ACKNOWLEDGMENT

The authors thank Dr. Saara M. Totterman, Director of the Magnetic Resonance Imaging Center at the University of Rochester Medical Center, for providing imaging time for this study.

## REFERENCES

1. B. Antalek and W. Windig, *J. Am. Chem. Soc.* **118,** 10,331–10,332 (1996).
2. W. Windig and B. Antalek, *Chemom. Intell. Lab. Syst.* **37,** 241–254 (1997).
3. M. Kubista, *Chemom. Intell. Lab. Syst.* **7,** 273–279 (1990).
4. I. Scarminio and M. Kubista, *Anal. Chem.* **65,** 409–416 (1993).
5. K. S. Booksh and B. R. Kowalski, *J. Chemom.* **8,** 287–292 (1994).
6. E. Sanchez and B. R. Kowalski, *Anal. Chem.* **58,** 496–499 (1988).
7. B. Wilson, E. Sanchez, and B. R. Kowalski, *J. Chemom.* **3,** 493–498 (1989).
8. E. O. Stejskal and J. E. Tanner, *J. Chem. Phys.* **42,** 288–292 (1965).
9. P. Geladi and H. Grahn, ''Multivariate Image Analysis,'' Wiley, New York (1996).
10. K. Esbensen and P. Geladi, *Chemom. Intell. Lab. Syst.* **7,** 67–86 (1989).
11. H. Grahn, N. M. Szeverenyi, M. W. Roggenbuck, and P. Geladi, *Chemom. Intell. Lab. Syst.* **7,** 87–93 (1989).
12. P. Geladi and K. Esbensen, *J. Chemom.* **5,** 97–111 (1991).
13. P. Geladi, H. Isaksson, L. Lindqvist, S. Wold, and K. Esbensen, *Chemom. Intell. Lab. Syst.* **5,** 209–220 (1989).
14. H. F. Grahn, N. M. Szeverenyi, M. W. Roggenbuck, F. Delaglio, and P. Geladi, *Chemom. Intell. Lab. Syst.* **5,** 311–322 (1989).
15. H. F. Grahn and J. Sääf, *Chemom. Intell. Lab. Syst.* **514,** 391–396 (1992).
16. L. M. Fletcher, J. B. Barsotti, and J. P. Hornak, *Magn. Reson. Med.* **29,** 623–630 (1993).
17. B. Antalek, J. P. Hornak, and W. Windig, *J. Magn. Reson.* **132,** 307–315 (1998).